

A Fast and Robust Matching Framework for Multimodal Remote Sensing Image Registration

Yuanxin Ye^{1*}, Lorenzo Bruzzone², Jie Shan³, Francesca Bovolo⁴ and Qing Zhu¹

¹Faculty of Geosciences and Environmental Engineering, Southwest Jiaotong University, Chengdu 610031, China.

²Department of Information Engineering and Computer Science, University of Trento, 38123 Trento, Italy

³School of Civil Engineering, Purdue University, West Lafayette, IN 47907, USA.

⁴Center for Information and Communication Technology, Fondazione Bruno Kessler, 38123 Trento, Italy

Declarations of interest: none

¹Abstract: While image registration has been studied in remote sensing community for decades, registering multimodal data [e.g., optical, light detection and ranging (LiDAR), synthetic aperture radar (SAR), and map] remains a challenging problem because of significant nonlinear intensity differences between such data. To address this problem, we present a novel fast and robust matching framework integrating local descriptors for multimodal registration. In the proposed framework, a local descriptor (such as Histogram of Oriented Gradient (HOG), Local Self-Similarity or Speeded-Up Robust Feature) is first extracted at each pixel to form a pixel-wise feature representation of an image. Then we define a similarity measure based on the feature representation in frequency domain using the Fast Fourier Transform (FFT) technique, followed by a template matching scheme to detect control points between images. We also propose a novel pixel-wise feature representation using orientated gradients of images, which is named channel features of orientated gradients (CFOG). This novel feature is an extension of the pixel-wise HOG descriptor, and outperforms that both in matching performance and computational efficiency. The major advantages of the proposed framework include (1) structural similarity representation using the pixel-wise feature description and (2) high computational efficiency due to the use of FFT. Moreover, we design an automatic registration system for very large-size multimodal images based on the proposed framework. Experimental results

¹ Corresponding author: Yuanxin Ye, e-mail: yeyuanxin@home.swjtu.edu.cn

obtained on many different types of multimodal images show the superior matching performance of the proposed framework with respect to the state-of-the-art methods and the effectiveness of the designed system, which show very good potential large-size image registration in real applications.

Keywords: image registration, multimodal remote sensing images, pixel-wise feature representation, FFT

I. Introduction

In recent years, geospatial information techniques have undergone a rapid development, and can acquire the diverse multimodal remote sensing data [e.g., Optical, infrared, light detection and ranging (LiDAR) and synthetic aperture radar (SAR)] and even topographic map data. Since these multimodal data can provide complementary information for Earth observation, they have been widely used in many applications such as land-cover and land-use analysis (Tuia et al., 2016), change detection (Bruzzone and Bovolo, 2013), image fusion (Zhang, 2004), damage monitoring (Brunner et al., 2010), etc. A key step to integrate multimodal data for these applications is image registration, which aligns two or more images captured by different sensors, at different times or from different viewpoints (Zitova and Flusser, 2003).

With modern remote sensing sensors, pre-registration can be achieved through direct georeferencing by applying physical sensor models and navigation devices such as global positioning (GPS) and inertial navigation (INS) systems. As a result, the obvious global geometric distortions (e.g., rotation and scale changes) can be removed by such pre-registration, which makes the images only have an offset of a few pixels (Bunting et al., 2010; Goncalves et al., 2012). The georeferencing information provides the convenience for the further precise registration. However, acquired at different spectral regions or by different sensors, multimodal images often have significant nonlinear intensity differences. Fig. 1 shows two pairs of multimodal images covering the same scenes, which include optical, SAR, and map data. Clearly, they have quite different intensity and texture patterns, even leading to the difficulty to detect control points (CPs) or correspondences by visual inspection. Therefore, the focus of this paper is to effectively address nonlinear intensity differences to achieve precise multimodal image registration.



(a)

(b)

Fig. 1. Examples of different intensity and texture patterns between multimodal images. (a) SAR (left) and optical (right) images. (b) Map (left) and optical (right) images.

Many automatic registration methods have been developed in the past decades for remote sensing images (see Section II). However, most of these methods only concentrate on the development of new techniques, and do not adequately consider the requirements of real applications. For example, most methods cannot effectively handle large-size images, and some of them usually ignore to use the georeferencing information to guide image registration. Today, popular commercial remote sensing software, such as ENVI and ERDAS, have already developed automatic image registration functions. Nevertheless, they are more on the registration of single-modal images and are vulnerable to multimodal registration. As a result, multimodal registration often requires manual intervention in practice, which is very time-consuming. Moreover, this may also bring some registration errors caused by human's subjectivity. Hence, a fast and robust automatic registration system for multimodal remote sensing images is highly desired in practice.

Recently, our studies have shown that structure and shape properties are preserved between different modalities (Ye et al., 2017b; Ye and Shen, 2016; Ye et al., 2017c; Ye et al., 2015) . According to this finding, we can detect CPs by computing similarity on structure and shape descriptors such as Local Self-Similarity (LSS) (Shechtman and Irani, 2007) and Histogram of Oriented Gradient (HOG) (Dalal and Triggs, 2005). In addition, the computer vision community usually uses pixel-wise descriptors to represent global structure and shape properties of images. Such kind of feature representation has been successfully applied to object recognition (Lazebnik et al., 2006), motion estimation (Brox and Malik, 2011), and scene alignment (Liu et al., 2011). Inspired by these developments, here we explore the pixel-wise feature representation for multimodal registration.

This paper presents a novel fast and robust matching framework for automatic registration of multimodal remote sensing images. We first extract a local descriptor [such as HOG, LSS or Speeded-Up Robust Feature (SURF) (Bay et al., 2008)] at each pixel of an image to generate the pixel-wise feature representation. Then a similarity measure based on the feature representation is built in the frequency domain, the computation of which is accelerated by using the fast Fourier transform

(FFT). Subsequently, a template matching scheme is employed to detect CPs between images. In addition, we also propose a novel pixel-wise feature representation using orientated gradients of images, which is named channel features of orientated gradients (CFOG). This novel feature is an extension of the pixel-wise HOG descriptor, and outperforms the former in both matching performance and computational efficiency. Finally, based on the proposed matching framework, we design a fast and robust registration system for multimodal images. This system takes into full account the characteristics of remote sensing data and the requirements of practical operation. It uses the georeferencing information to guide image registration, and can process large-size multimodal images (i.e., images with more than 20000×20000 pixels). Accordingly, the main contributions of this paper consist of:

- 1) A fast and robust matching framework integrating local descriptors for the automatic registration of multimodal remote sensing images. The framework evaluates similarity between images based on the pixel-wise feature representation, and accelerates image matching by using the FFT technique in frequency domain. It is a general framework and can integrate different kinds of local descriptors for image matching.
- 2) A novel pixel-wise feature representation named CFOG using orientated gradients, which is an extension of the pixel-wise HOG descriptor.
- 3) An automatic registration system for large-size multimodal remote sensing images based on the proposed matching framework.

This paper extends our early works (Ye, 2017; Ye et al., 2017a) by adding a detailed principled derivation of the proposed framework and proposing a novel pixel-wise descriptor named CFOG. We also perform the more thorough evaluation for the proposed framework using more multimodal remote sensing data.

The rest of this paper is organized into six sections. Section II reviews the related work on multimodal remote sensing image registration. Section III describes the proposed fast and robust matching framework, and Section IV presents its implementation in an automatic registration system. Section V analyzes the performance of the proposed matching framework

using various multimodal datasets, while Section VI evaluates the designed registration system using a pair of large-size multimodal images. Section VII concludes on the findings and significance of this work.

II. Related Work

This section briefly reviews two groups of registration methods for multimodal remote sensing images: feature-based and intensity-based methods.

Feature-based methods first extract image features, and then match them based on their similarities. The extracted features should be highly distinct, stable, and repeatable between images. They can be points (Huo et al., 2012; Yu et al., 2008), contours or edges (Chen and Shao, 2013; Li et al., 1995; Shi and Shaker, 2006), regions (Goncalves et al., 2011). Recently, local invariant features have a rapid development in computer vision community, and have got considerable attention from researchers in remote sensing. Some famous local invariant features, such as the scale-invariant feature transform (SIFT) (Lowe, 2004), SURF, and shape context (Belongie et al., 2002), have been applied to remote sensing image registration (Bouchiha and Besbes, 2013; Fan et al., 2013; Huang and Li, 2010). Although these features are robust to scale, rotation and linear intensity changes, they are vulnerable to nonlinear intensity differences. To improve their matching performance, researchers proposed some improved local features such as the uniform robust SIFT (Sedaghat et al., 2011), the adaptive binning SIFT (Sedaghat and Ebadi, 2015), and the scale restricted SURF (Teke and Temizel, 2010). However, these improved features still cannot effectively handle multimodal remote sensing registration. The main problem of these feature-based methods is that they rely on extracting highly repeatable features between images. More precisely, the features extracted in an image should be detected in the other image when using the same feature extraction algorithm. Only in that way it is possible to achieve enough corresponding features for image matching. Due to large discrepancies in intensity and texture, the extracted features between multimodal images usually have a low repeatability (Gesto-Diaz et al., 2017; Kelman et al., 2007), which substantially degrades the matching performance.

Intensity-based methods achieve image registration through image matching, which evaluates the similarity of corresponding

window pairs in two images, and select the one with the maximum similarity as the correspondence (Ma et al., 2015). During this process, the correspondence detection can be computed in either the spatial or frequency domain.

In the spatial domain, common similarity measures include the sum of squared differences (SSD), the normalized correlation coefficient (NCC), and the mutual information (MI). SSD evaluates similarity by directly comparing the differences of image intensity values. Though SSD is simple and fast for computation, it is sensitive to noise and intensity differences (Zitova and Flusser, 2003). As a classic similarity measure, NCC has been commonly applied to the registration of remote sensing images due to its invariance to linear intensity variations (Ma et al., 2010; Uss et al., 2016). However, NCC is not well adapted to the registration of multimodal images with complex intensity changes. MI describes the statistical dependency between images, which is very weak related to the functional relationship between intensities. As a result, MI can address nonlinear intensity differences (Hel-Or et al., 2014; Xu et al., 2016). Recent studies also showed that MI is suitable for multimodal remote sensing image registration (Chen et al., 2003; Cole-Rhodes et al., 2003; Suri and Reinartz, 2010). However, the main drawback of MI is that it ignores the spatial information of neighboring pixels, which deteriorates the quality of image alignment (Fan et al., 2010). In addition, the high computational cost is another limitation for MI extensive application in remote sensing image registration (Hel-Or et al., 2014).

In the frequency domain, the most popular similarity measure is phase correlation (PC), which can quickly estimate the translations between images based on the Fourier shift theorem (Bracewell and Bracewell, 1986). Nowadays, PC has been extended to account for scale and rotation changes (Reddy and Chatterji, 1996), and also applied to remote sensing image registration (Wan et al., 2016; Wan et al., 2015). Compared with the spatial measures, its main advantage is the high computational efficiency (Wong and Orchard, 2008). Nonetheless, PC cannot effectively address the registration of multimodal images with significant intensity differences. This is because that PC evaluates similarity by using intensity information of images as well as the spatial measures.

Recently, some hybrid approaches combined feature- and intensity-based methods. These approaches achieve correspondences by using the matching scheme of intensity-based methods (i.e., template matching) to perform similarity evaluation on image

features rather than intensities. As such, avoiding to extract the independent features between images, these approaches apply the intensity-based similarity measures on feature descriptors (e.g., gradients and wavelets) for image registration (Murphy et al., 2016; Ravanbakhsh and Fraser, 2013; Zavorin and Le Moigne, 2005). Moreover, the medical image processing community is also devoted to addressing multimodal registration by evaluating similarity on the dense structure and shape feature representations, which are built by extracting local descriptors at each pixel of an image (Heinrich et al., 2012; Li et al., 2016; Rivaz et al., 2014). Compared with the traditional feature- and intensity-based methods, these hybrid approaches improve registration accuracy. Inspired by these recent efforts, this paper intends to build a fast and robust matching framework based on the pixel-wise feature representation for multimodal remote sensing registration, and develop an automatic registration system for large-size remote sensing images.

III. Proposed Image Matching Framework

This section presents a fast and robust matching framework for the registration of multimodal remote sensing images. It captures the distinctive image structures by the pixel-wise feature representation. The similarity of the feature representations is evaluated by using a fast similarity measure built in the frequency domain. The CPs between images are then detected by a template matching scheme.

A. Motivation

Our previous work found that HOG is robust to nonlinear intensity differences between images, and can be successfully applied to the registration of multimodal images (Ye et al., 2017b). HOG can effectively depict the structure and shape properties by the distribution of gradient magnitudes and orientations within local image regions. To construct this descriptor, a template window is first divided into some overlapping blocks, which consist of $m \times m$ cells, each containing several pixels. Then a local histogram of the quantified gradient orientations is computed using all the pixels of each block. Finally, the histogram of each block is collected at a stride of a half block width to generate the HOG descriptor. Fig. 2 shows the fundamental structure of HOG.

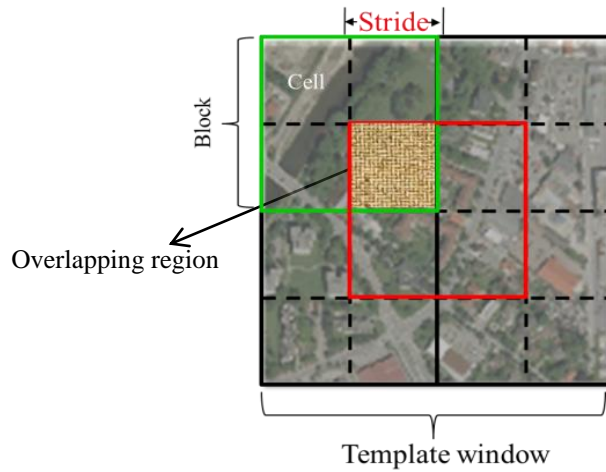


Fig. 2 Fundamental structure of HOG

We intend to show below that the matching performance of HOG can be improved by decreasing the stride between adjacent blocks. To illustrate that, a pair of optical and SAR images is used and the similarity is evaluated by using the SSD of HOG. Fig. 3 plots the SSD similarity curves of HOG with the different strides, where the template size for computing HOG is 40×40 pixels, and the search window for detecting CPs is 20×20 pixels. One can see that the matching errors become smaller and the similarity curves are smoother when the stride decreases, which means that HOG can present the optimal matching performance when it is computed at each pixel (i.e., stride = 1 pixel). Apart from HOG, other local descriptors (such as LSS and SURF) also present a similar phenomenon for multimodal matching.

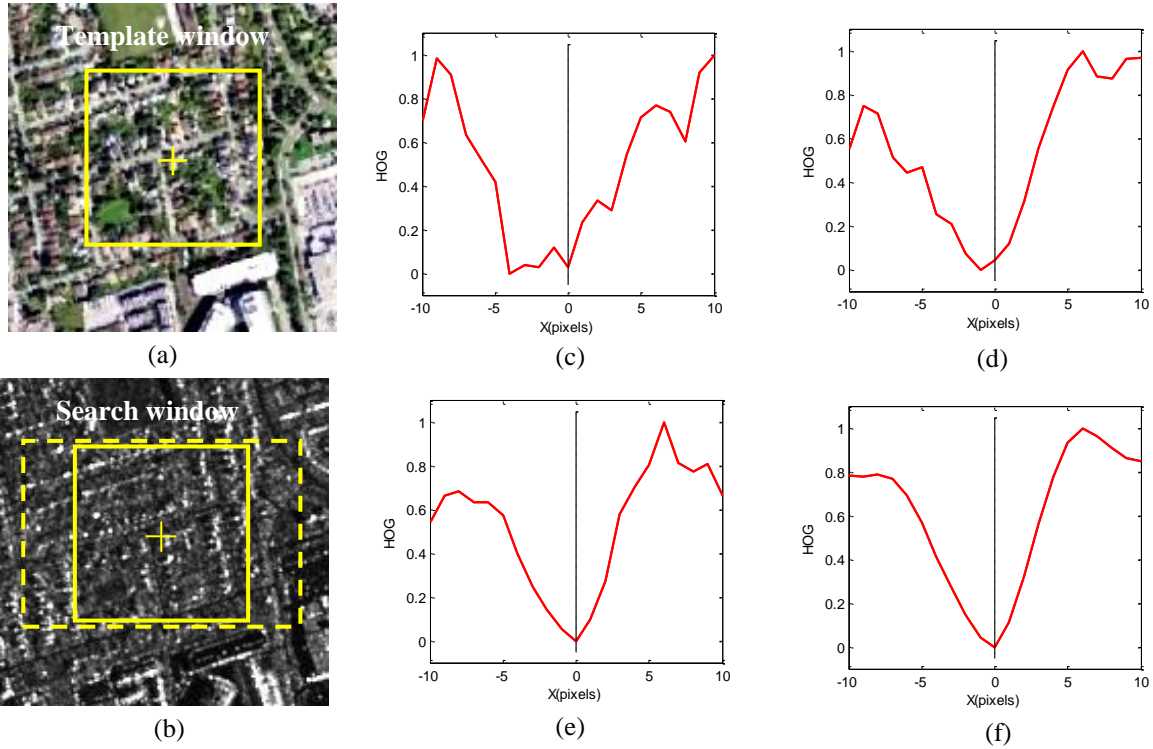


Fig. 3 SSD similarity curves of HOG with different strides between adjacent blocks. (a) Optical image. (b) SAR image. (c) Similarity curve with stride = 8 pixels. (d) Similarity curve with stride = 4 pixels. (e) Similarity curve with stride = 2 pixels. (h) Similarity curve with stride = 1 pixel.

B. Pixel-wise feature representation

The proposed matching framework is based on a pixel-wise feature representation. Such pixel-wise feature representation forms a 3D image since each pixel has a feature vector with a certain dimension (see Fig. 4). In this paper, some popular local descriptors, such as HOG, LSS, SURF are integrated into the proposed framework for multimodal matching. In addition, we also propose a novel pixel-wise feature representation named CFOG, which is an extension of the pixel-wise HOG descriptor. Below, we present the implementation details for the descriptors used in the proposed framework.

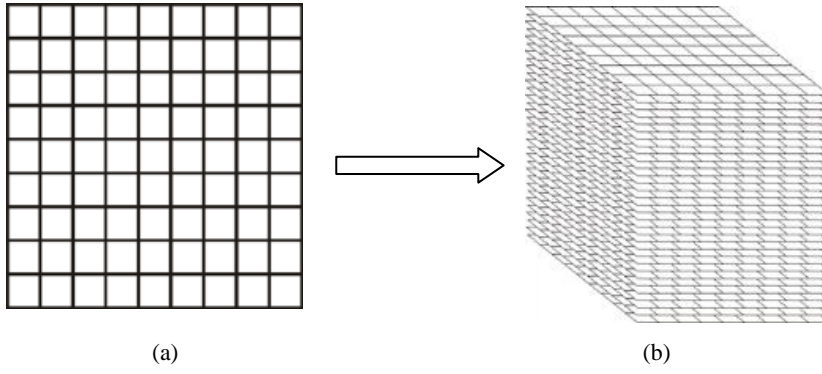


Fig. 4 Pixel-wise structural feature representation. (a) Image. (b) 3D feature representation

C. HOG

The traditional HOG descriptor is computed by dividing an image into overlapping blocks and collecting the descriptors of each block to form the final feature vector. Since our matching framework requires calculating the descriptor at each pixel, it is necessary to define a block region centered on each pixel and extract the HOG descriptor. For each pixel, the HOG descriptor is a 3D histogram computed from the block region consisting of 2×2 cells, where the gradient direction is quantized into 9 orientation bins. Accordingly, this descriptor has $2 \times 2 \times 9 = 36$ histogram bins in total, where each pixel of the block contributes to the histogram bins depending on its spatial location and gradient orientation (Tola et al., 2010). The weight of contribution is proportional to its gradient magnitude. To avoid boundary effects, each pixel contributes to its adjacent histogram bins by trilinear interpolation. Finally, this descriptor is normalized by the L2 norm to achieve the robustness to intensity changes.

D. LSS

LSS is a feature descriptor that captures internal geometric layouts of local self-similarities within images (Shechtman and Irani, 2007). In order to extract the pixel-wise feature descriptor, we define a local region centred at each pixel of an image, and extract its LSS descriptor. Fig. 5 shows the processing chain of the LSS descriptor formation of a local region. In this region, all surrounding image patch p_i are compared with the patch centered at q using the SSD between the patch intensities. Then, the $SSD_q(x, y)$ is normalized and transformed into a “correlation surface” $S_q(x, y)$.

$$S_q(x, y) = \exp\left(-\frac{SSD_q(x, y)}{\max(var_{nosie}, var_{auto}(q))}\right) \quad (1)$$

where var_{nosie} is a constant which corresponds to acceptable photometric changes (in intensities or due to noise). $var_{auto}(q)$

accounts for the patch contrast and its pattern structure.

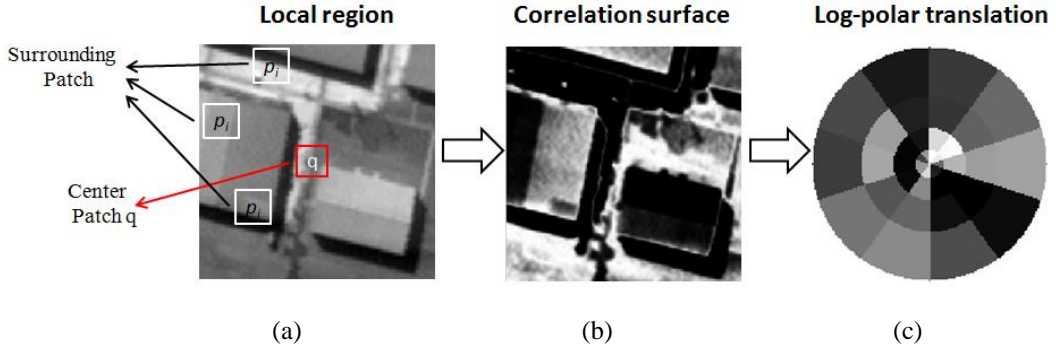


Fig. 5 Processing chain of the LSS descriptor formation. (a) Local image region, (b) Correlation surface of (a), (c) Final LSS descriptor.

The correlation surface $S_q(x, y)$ is then transformed into a log-polar coordinate system and partitioned into some bins, where the maximal correlation value of each bin is used as the entry to generate the LSS descriptor associated with the pixel q . Finally, the LSS descriptor is linearly stretched to the range of [0,1] to achieve better robustness to intensity variations.

E. SURF

SURF is a local feature which includes a feature detection and a feature description phase. The feature detection is to extract interesting points that have the scale and predominant orientation. Since our work focuses on roughly upright scaled multimodal images (i.e., no obvious scale and rotation changes between images), we skip this step and use the Upright SURF descriptor (named U-SURF) to compute the pixel-wise feature representation. For each pixel of an image, we define a block region to compute its U-SURF descriptor. This block region is divided into 4×4 sub-regions, each of which contains 5×5 pixels. For each sub-region, we generate the descriptor by computing the horizontal and the vertical Haar wavelet responses (named dx and dy , respectively) on integral images (Viola and Jones, 2001). The dx and dy are summed up in each sub-region to form the final U-SURF feature vector $v = (\sum dx, \sum dy, \sum |dx|, \sum |dy|)^T$. It should be noted that the intensities are sometimes inverse between multimodal images, which results in $\sum dx$ and $\sum dy$ vulnerable to this intensity distortions. Therefore, we only use $v' = (\sum |dx|, \sum |dy|)^T$ to generate a simplified U-SURF descriptor (see Fig. 6).

The simplified U-SURF descriptor is not only more robust for multimodal matching, but also is more computationally

effective than the original version. This is because its dimension (32 elements) is smaller than that of the original one (64 elements).

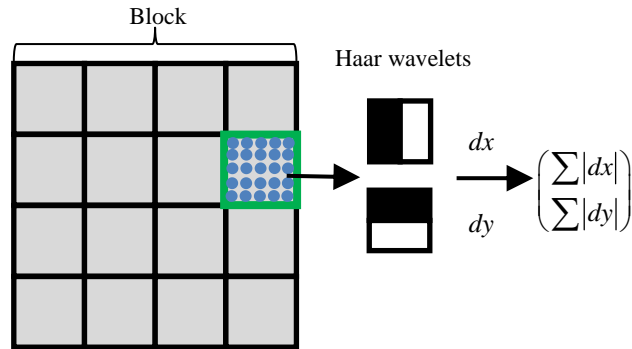


Fig. 6 To build the simplified SURF descriptor, a block region is defined centred around each pixel, and it is divided into 4×4 sub-regions, each of which consists of 5×5 pixels. For each sub-region, we collect the sums $\sum |dx|$ and $\sum |dy|$.

F. CFOG

CFOG is inspired by HOG. As mentioned above, HOG is a 3D histogram based on gradient magnitudes and orientations of a block region. This histogram is weighted by a trilinear interpolation method, which results in that each histogram bin contains the weighted sum of gradient magnitudes around its center. This interpolation procedure is time-consuming because it requires computing the weights of each pixel for both the spatial and orientation bins. Moreover, as one block region usually includes multiple cells, we first need to compute the histogram for each cell, and then collect them to form the final descriptor. Thus, by reducing the number of cells in one block we can raise the computational efficiency. In addition, we found that the HOG descriptor shows no obvious performance degradation in the proposed matching framework when it is extracted from a one-cell block instead of a multi-cell block. Hence, the pixel-wise feature representation can be built by using the HOG descriptor with a one-cell block. Note that the trilinear interpolation in a one-cell block can be regarded as a convolution operation with a triangular kernel, which can be efficiently computed at each pixel of an image (Tola et al., 2010). This is because the convolution computes the histogram only once per block, and reuses them for all pixels. Therefore, we reformulate the HOG descriptor by the convolution in image gradients of specific orientations. The convolution is performed by a Gaussian kernel instead of a triangular kernel, since the former is more effective to suppress noise and reduce

the contribution of the gradient far from the region center. This reformulated descriptor is named CFOG. It presents a similar invariance as the HOG descriptor, but is more computationally efficient for building a pixel-wise feature representation. In addition, it has a smaller descriptor dimensionality, which is beneficial for fast image matching.

We now give a formal definition for the proposed CFOG. For a given image, we first compute its m orientated gradient channels, which are referred as to g_i , $1 \leq i \leq m$. Each orientated gradient channel $g_o(x, y)$ is the gradient magnitude located at (x, y) for the quantized orientation o if it is larger than zero, else its value is zero. Formally, an orientated gradient channel is written as $g_o = \lfloor \partial I / \partial o \rfloor$, where I is the image, o is the orientation of the derivative, and $\lfloor \cdot \rfloor$ denotes that the enclosed quantity is equal to itself when its value is positive or zero otherwise. In practice, we do not need to compute g_o for each orientation separately, while instead it is computed by using the horizontal and vertical gradients (named g_x and g_y , respectively) according to the following equation:

$$g_\theta = \lfloor \text{abs}(\cos \theta \cdot g_x + \sin \theta \cdot g_y) \rfloor \quad (2)$$

where, θ is the quantized gradient orientation. abs represents the absolute value, which can transfer the gradients from $[180^\circ, 360^\circ)$ to $[0^\circ, 180^\circ)$ to handle the intensity inversion between multimodal images.

After the formation of the orientated gradient channel, it is convolved using a 3D Gaussian-like kernel to achieve the convolved feature channel as $g_o^\sigma = g_o * \lfloor \partial I / \partial o \rfloor$, where σ is the standard deviation (STD) of the Gaussian kernel. Strictly speaking, this kernel is not a 3D Gaussian function in the 3D space, but a 2D Gaussian kernel in X- and Y-directions and a kernel of $[1, 2, 1]^T$ in the gradient orientation direction (hereinafter referred to as Z-direction). The Z-direction convolution smoothes the gradients in the orientation direction, which can reduce the influence of orientation distortions caused by local geometric and intensity deformations between images.

The convolved feature channel is the proposed CFOG, which is a 3D pixel-wise feature representation and can capture the structural properties of images. Fig. 7 shows the processing chain of CFOG. CFOG can be regarded as an extension of HOG because its pixel value is similar to the value of a bin in HOG, which is a weighted gradient magnitude computed over a local region. The main difference between the two descriptors is that CFOG uses the 3D Gaussian-like convolution to build

the histogram, whereas HOG depends on the time-consuming trilinear interpolation method.

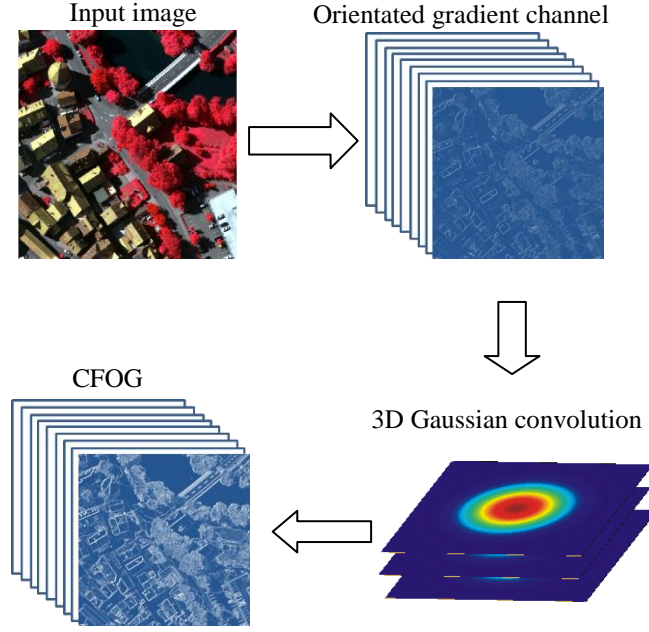


Fig. 7 Processing chain of CFOG.

G. Proposed similarity measure

This subsection introduces a similarity measure for template matching based on the 3D pixel-wise feature representation, and its fast computation by using FFT.

It is generally known that SSD is a popular similarity measure for image matching. Given a reference image and a sensed image, let their corresponding pixel-wise feature representations be D_1 and D_2 , respectively. The SSD between the two feature representations within the template window i in the D_1 is defined as.

$$S_i(v) = \sum_x [D_1(x) - D_2(x-v)]^2 T_i(x) \quad (3)$$

where x is the location of a pixel in a 3D feature representation, and $T_i(x)$ is the masking function over $D_1(x)$, where $T_i(x) = 1$ within the template window and $T_i(x) = 0$ otherwise. $S_i(v)$ is the SSD similarity function between D_1 and D_2 translated by a vector v over a template window i . By minimizing the $S_i(v)$, we can achieve the match between D_1 and D_2 . Accordingly, the matching function is defined as

$$v_i = \arg \min_v \left\{ \sum_x [D_1(x) - D_2(x-v)]^2 T_i(x) \right\} \quad (4)$$

Where, the obtained translation v_i is a translation vector that matches D_1 with D_2 given the template window i .

Since the pixel-wise feature representation is a 3D image with large-volume data, it is time consuming to exhaustively compute the SSD similarity function for all candidate template windows. This is an intrinsic problem for template matching, as a template window needs to slide pixel-by-pixel within a search region for detecting correspondences. An effective approach to reduce the computation is to use the FFT technique for acceleration.

At first, the SSD similarity function presented in Equation (3) can be expanded as

$$S(v_i) = \sum_x D_1^2(x)T_i(x) + \sum_x D_2^2(x-v)T_i(x) - 2\sum_x D_2(x-v) \cdot D_1(x)T_i(x) \quad (5)$$

since the first term is a constant, the similarity function $S_i(v)$ can achieve the match by minimizing the operation of the last two terms. Furthermore, the last two terms can be regarded as convolutions, and their computation can be accelerated using FFT since convolutions in the spatial domain become dot products in the frequency domain. Hence, the translation vector v_i can be computed by

$$v_i = \arg \min_v \left\{ F^{-1} \left[F^*(D_2)F(D_2T_i) \right](v) - 2F^{-1} \left[F^*(D_2)F(D_1T_i) \right](v) \right\} \quad (6)$$

Where, F and F^{-1} denote the forward and inverse FFTs, respectively, and F^* is the complex conjugate of F . The computation of the similarity function can be significantly reduced by using (6). For example, given a template window with a size of $N \times N$ pixels and its search region is $M \times M$ pixels, the SSD takes $O(M^2N^2)$ operations, while the proposed approach takes $O\left((M+N)^2 \log(M+N)\right)$ operations. This approach reduces more computation efficiency for larger template windows or search regions (e.g., more than 20×20 pixels).

In the proposed framework, CFOG, HOG, LSS, and SURF are integrated as the similarity measures by (6). They are named CFOG, FHOG, FLSS, and FSURF respectively. To illustrate their advantages to match multimodal images, they are compared with NCC and MI by the similarity maps. Two pairs of multimodal images are used in the test. One is a pair of optical and infrared images with a high resolution, and the other is a pair of optical and SAR images with a high resolution.

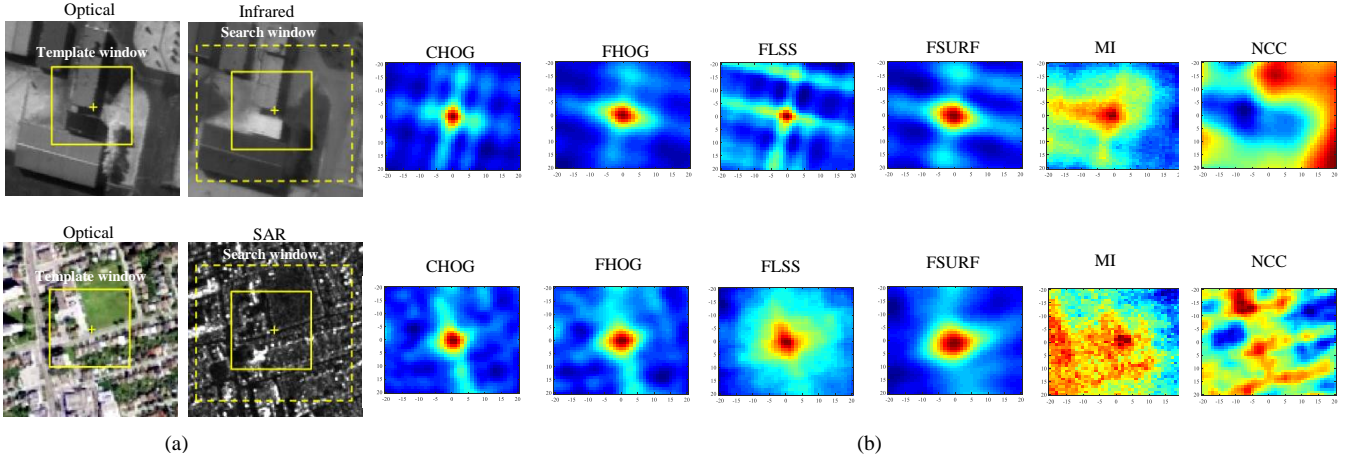


Fig. 8 Similarity maps of CFOG, FHOG, FLSS, FSURF, MI and NCC for the optical-to-infrared and optical-to-SAR image pairs, where the template window is 60×60 pixels, and the search window is 20×20 pixels. In each map, the center of the map corresponds to the correct match location. (a) Test data. (b) Similarity maps.

Fig. 8 shows the similarity maps of these similarity measures. One can see that NCC fails to detect the correspondences because of the significant intensity differences. MI finds the correct match for the optical and infrared images, but it has a few location errors for the optical and SAR images. Moreover, the similarity maps of MI look quite noisy. In contrast, the proposed similarity measures, i.e., CFOG, FHOG, FLSS, and FSURF, present smoother similarity maps with sharp peaks, and achieve correct matches for both cases. This preliminarily indicates that the proposed similarity measures are more robust than the others for multimodal matching. A more detailed analysis of their performance will be given in Section V.

IV. Registration system based on the proposed matching framework

This section presents an automatic registration system for multimodal images based on the proposed matching framework. It uses CFOG as the similarity measure for image matching because it performs better than the others in our experiments (See Section V-E). Since remote sensing images are often very large in size, it is not preferable to read the entire image into memory. Considering that the georeferencing information of images can be used to predict the search region for CP detection, the designed system employs a partition strategy for image matching. More precisely, we first divide an image into some non-overlapping regions, and then perform CP detection by only using a small portion of image data in each

region. The designed system is developed with C++, which includes the following steps: feature point detection, feature point matching, outlier rejection, and image rectification.

Feature point detection: The Harris operator is used to detect the dense and evenly distributed feature points in the reference image. We first divide the image into $n \times n$ regularly spaced grids, and input an image chip (60×60 pixels) to the memory centred on each grid intersection. In the image chip, we compute the Harris value for each pixel, and select k pixel points with the largest Harris values as the feature points. As a result, $n \times n \times k$ feature points can be extracted in the reference image, where the values of n and k are decided by users.

Feature point matching: Once a set of feature points are detected in the reference image, a search region in the sensed image is determined based on the georeferencing information. Subsequently, the proposed framework is employed to achieve CPs between images.

Outlier rejection: In the above image matching, outliers (i.e., CPs with large errors) are inevitable because of some occlusions such as clouds and shadow. These outliers are removed through the following iterative rejection procedure: (1) Establish a geometric mapping model using all the CPs; (2) Calculate the residuals and root mean square errors (RMSEs) of CPs by the least square method, and remove the CP with the largest residual; (3) Repeat the above procedure until the RMSE is smaller than a given threshold (e.g., 1 pixel). In the rejection procedure, the choice of the mapping model depends on geometric distortions between images. The designed system uses a cubic polynomial model for outlier rejection because this model is more effective to prefit non-rigid geometric deformation than other models (such as the first and second polynomial models) (Ye and Shan, 2014).

Image rectification: Large-size remote sensing images usually cover mixed terrains such as plains, mountains and buildings, which cause significant local distortions between images. To address that, the system employs a piecewise linear model for image rectification. This model is based on triangulated irregular networks (TINs), which divide the image into triangular regions. In each region, an affine transformation model is estimated and applied for rectification.

V. Experimental Results: Performance of The Proposed Matching Framework

This section evaluates the performance of the proposed matching framework with different types of multimodal remote sensing data. Moreover, some state-of-the-art similarity measures, such as NCC, MI, and HOG_{ncc} (Ye et al., 2017b), are used for comparisons. In order to make a fair comparison, the parameters of all the similarity measures are also tuned by using the same datasets. For each similarity measure, its optimal parameters are used in the following comparative experiments. The datasets, evaluation criteria, implementation details, and experimental results are presented in the following.

A. Datasets

Ten matching cases are used to analyze the performance of the proposed framework. These cases consist of various multimodal image pairs, including optical-to-infrared (cases 1, 2), LiDAR-to-optical (cases 3, 4, 5), optical-to-SAR (cases 6, 7, 8), and optical-to-map (cases 9,10). These test image pairs are acquired at different times, and exhibit diverse land covers such as urban, suburb, agriculture, rivers, and flat areas. In general, the matching of optical-to-SAR and optical-to-map is more difficult than the other cases because there is a significant speckle noise in the SAR images, and some text labels on the maps. TABLE I gives the detailed description of each case, and Fig. 9 shows the test image pairs. The two images of each pair have been pre-registered by using metadata or physical sensor models, and resampled to the same ground sample distance (GSD), resulting in no obvious translation, rotation, and scale differences. Nonetheless, significant intensity and texture differences exist between the images.

TABLE I
DETAILED DESCRIPTION OF TEST CASES

| Category | Case | Dataset description | | |
|---------------------|------|---|---|--|
| | | Reference image | Sensed image | Image characteristic |
| Optical-to-infrared | 1 | Sensor: Daedalus optical GSD: 0.5m Date: 04/2000 Size: 512×512 | Sensor: Daedalus infrared GSD: 0.5m Date: 04/2000 Size: 512×512 | Images cover a urban area with buildings |
| | 2 | Sensor: Landsat 5 TM band 1 GSD: 30m Date: 09/2001 Size: 1074×1080 | Sensor: Landsat 5 TM band 4 GSD: 30m Date: 03/2002 Size: 1074×1080 | Images cover a suburb area, and have a temporal differences of 6 months |
| LiDAR-to-optical | 3 | Sensor: LiDAR intensity GSD: 2 m Date: 10/2010 Size: 600×600 | Sensor: WorldView 2 optical GSD: 2 m Date: 10/2011 Size: 600×600 | Images cover an urban area with high buildings, and have local geometric distortions, and a temporal difference of 12 months. Moreover, there is the obvious |

| | | | | |
|----------------|---|---|---|---|
| Optical-to-SAR | 4 | Sensor: LiDAR intensity GSD: 2 m Date: 10/2010 Size: 621×617 | Sensor: WorldView 2 optical GSD: 2 m Date: 10/2011 Size: 621×621 | noise on the LiDAR intensity image. |
| | 5 | Sensor: LiDAR depth GSD: 2.5 m Date: 06/2012 Size: 524×524 | Sensor: Airborne optical GSD: 2.5 m Date: 06/2012 Size: 524×524 | Images cover an urban area with high buildings, and have local geometric distortions. Moreover, there is the obvious noise on the LiDAR depth image. |
| | 6 | Sensor: TM band3 GSD: 30m Date: 05/2007 Size: 600×600 | Sensor: TerraSAR-X GSD: 30m Date: 03/2008 Size: 600×600 | Images cover a plain area, and have a temporal difference of 10 months. Moreover, there is a significant noise on the SAR image. |
| | 7 | Sensor: Google Earth GSD: 3m Date: 11/2007 Size: 528×524 | Source: TerraSAR-X GSD: 3m Date: 12/2007 Size: 534×524 | Images cover an urban area with high buildings, and have and local geometric distortions. Moreover, there is the significant noise on the SAR image. |
| Optical-to-map | 8 | Sensor: Google Earth GSD: 3m Date: 03/2009 Size: 628×618 | Source: TerraSAR-X GSD: 3m Date: 01/2008 Size: 628×618 | Images cover an urban area with high buildings, and have local geometric distortions and a temporal difference of 14 months. Moreover, there is a significant noise on the SAR image. |
| | 9 | Sensor: Google Maps GSD: 0.5m Date: unknow Size: 700×700 | Sensor: Google Maps GSD: 0.5m Date: unknow Size: 700×700 | Images cover an urban area with high buildings, and have local geometric distortions. Moreover, there are some text labels on the SAR image. |
| 10 | Sensor: Google Maps GSD: 1.5m Date: unknow Size: 621×614 | Sensor: Google Maps GSD: 1.5m Date: unknow Size: 621×614 | | |

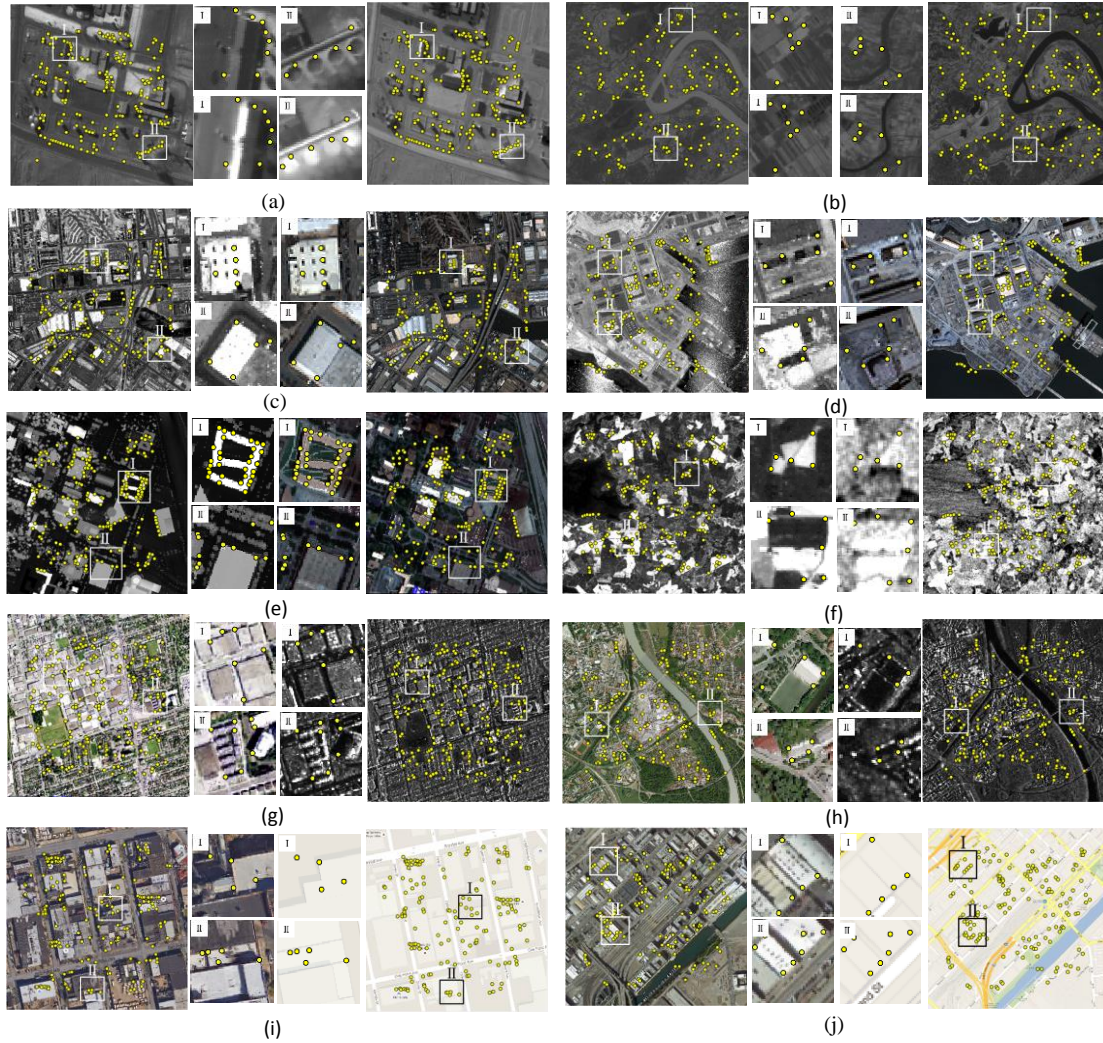


Fig. 9 CPs detected by CFOG with the template size of 100×100 pixels for all the test cases. (a) Case 1. (b) Case 2. (c) Case 3. (d) Case 4. (e) Case 5. (f) Case 6. (g) Case 7. (h) Case 8. (i) Case 9. (j) Case 10.

B. Evaluation criteria and implementation details

In our experiments, the precision and computational efficiency are used to analyze the performance of the proposed framework. The precision represents the ratio between the number of correct matches and the total numbers of matches, which is expressed as $precision = correct\ matches / total\ matches$. Considering that the matching performance of similarity measures is related to template sizes, we use template windows with different sizes to detect CPs between images.

The template matching starts with the block-based Harris operator to detect 200 evenly distributed feature points in the reference image. The CPs are achieved within a search region of 20×20 pixels in the sensed image. Subsequently, the sub-pixel accuracy of each CP is determined by a local fitting technique based on a quadratic polynomial (Ma et al.,

2010). In order to determine the number of correct CPs, we estimate a projective mapping model for each image pair by selecting 50 check points distributed evenly over the images. This estimated projective model is used to calculate the location error of each CP, and the CPs with location error smaller than 1.5 pixels are regarded as the correct ones. Since it is difficult to find accurate check points across modalities by manual selection, the check points are determined in the following way. Firstly, we use a large template size (200×200 pixels) to detect 200 CPs between the images by CFOG. This is because our experiments show that the similarity measure presents a higher precision value than the others; the larger template size, the higher its precision value. Then the outliers are removed by the iterative rejection procedure described in Section VI, and the 50 CPs with the least errors are selected as the final check points.

C. Analysis of Noise Sensitivity

This subsection examines the performance of the proposed similarity measures (i.e., CFOG, FHOG, FLSS, and FSURF) and the others by adding Gaussian white noise to the images. All the similarity measures are used to detect CPs with a template size of 80×80 pixels, and the average precision is used to analyze the noise sensitivity. This test is performed on the 10 pairs of real optical and infrared image with nonlinear intensity differences. For each pair, we add the Gaussian white noise with mean 0 and variance v in the range $[0, 1\%]$ to the infrared image, to generate a series of images with noise.

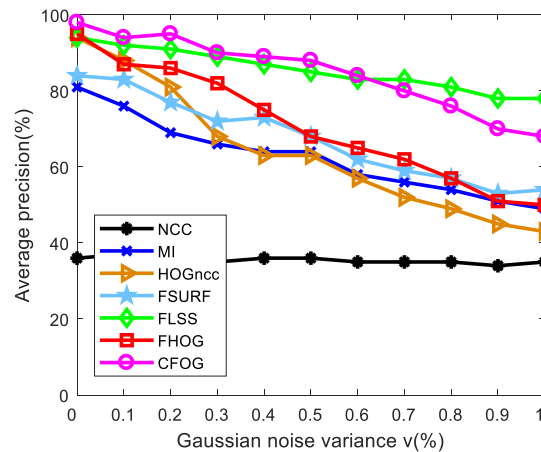


Fig. 10 Average precision values of similarity measures versus the various Gaussian noise.

Fig. 10 shows the average precision values of all the similarity measures versus the various Gaussian noise. FLSS and CFOG perform better than the others under increased noise, followed by FHOG and FSURF. Although MI presents stable results

under the various noise conditions, its average precision values are always smaller than these of our similarity measures. With regard to the three similarity measures based on the gradient orientation histogram, CFOG outperforms FHOG and HOG_{ncc} because it distributes gradient magnitudes into the orientation histogram by the Gaussian kernel, which is more effective to suppress the Gaussian noise than the trilinear interpolation used for FHOG and HOG_{ncc} .

D. Precision Analysis

Fig. 11 shows the comparative results of the seven similarity measures on all the ten test cases in terms of precision. In general, one can see that the proposed similarity measures (i.e., CFOG, FHOG, FLSS, and FSURF) outperform the intensity-based similarity measures (i.e., NCC, MI) in almost all the cases. This confirms that the proposed matching framework is effective for multimodal matching. NCC presents the worst performance because it is vulnerable to nonlinear intensity changes. Though MI performs better than NCC, it cannot effectively handle the matching of these multimodal images. Moreover, the performance of MI is sensitive to the template size compared with our similarity measures. As shown in Fig. 11(e)-(h), the precision values of MI are usually low for small template sizes (such as less than 44×44 pixels).

As the proposed similarity measures are constructed by different local descriptors, they present different performance in different test cases. CFOG and FHOG perform better and more steadily than FLSS and FSURF in most cases, which shows that the descriptors based on the gradient orientation histogram are more effective compared with the other descriptors for forming the pixel-wise feature representations to address the nonlinear intensity differences between the multimodal images. In addition, it can be observed that the precision values of FLSS are seriously affected by the characteristics of images. For cases 5, 9 and 10 where the LiDAR depth and map images are textureless [see Fig. 9(e), (i), (j)], FLSS has a significant performance degradation compared with the others. This indicates that the descriptor forming FLSS (i.e., LSS) cannot effectively capture the informative features for multimodal matching in textureless areas. Despite exhibiting a stable performance, FSURF achieves lower precision values than CFOG, FHOG, and FLSS in the most test cases. This may be attributed to the fact that the SURF descriptor is built by using the Haar wavelets, which are essentially filters used to calculate

gradient magnitudes in x- and y-directions. Thus this descriptor ignores gradient orientations that are more robust to complex intensity changes than gradient magnitudes (Fitch et al., 2002).

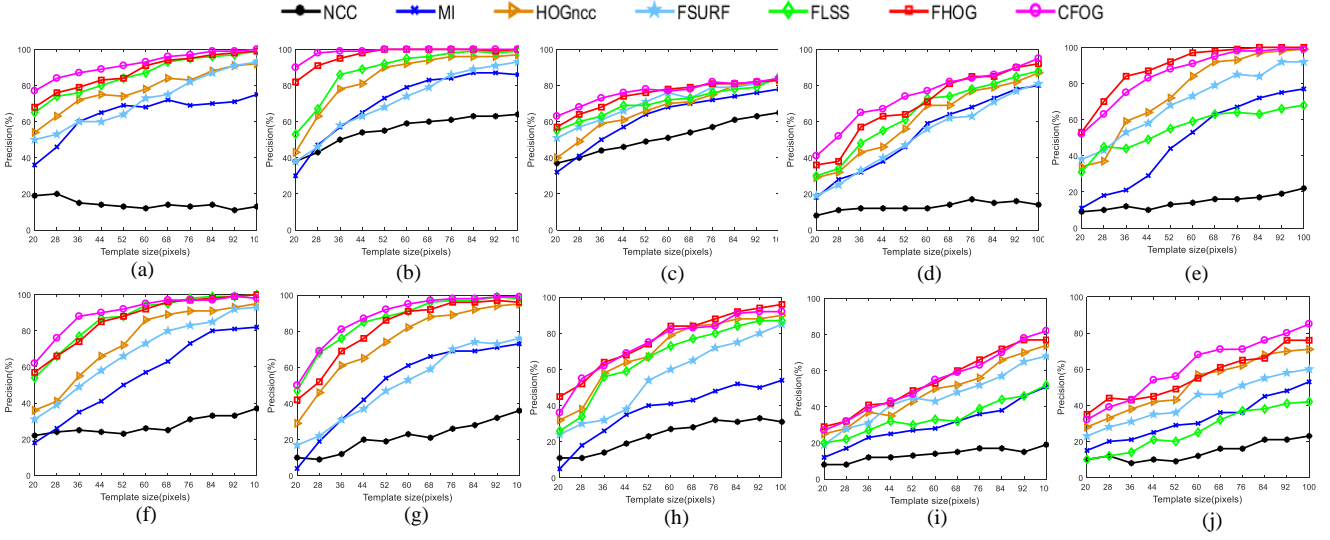


Fig. 11 Precision values of all the similarity measures versus the template size. (a) Case 1. (b) Case 2. (c) Case 3. (d) Case 4. (e) Case 5. (f) Case 6. (g) Case 7. (h) Case 8. (i) Case 9. (j) Case 10.

Let us compare the three similarity measures (i.e., CFOG, FHOG, and HOG_{ncc}) on the basis of the gradient orientation histogram. HOG_{ncc} achieves lower precision values than CFOG and FHOG for any template size in all the test cases. This is because HOG_{ncc} extracts the feature based on the relatively sparse sampled grids in an image, whereas CFOG and FHOG construct the denser feature representation by computing the descriptors for every pixel of the image, which can capture the local structure and shape properties of images more effectively and precisely. CFOG performs slightly better than FHOG. This may be because CFOG is more robust to noise compared with FHOG (see Section V-D). In addition, CFOG smoothes the histogram in the orientation direction, which can reduce the effects of orientation distortions caused by local geometric and intensity differences between images. Fig. 9 shows the CPs achieved by CFOG with the template size of 100×100 pixels for all cases. It can be clearly observed that these CPs are located in the correct positions.

All above results illustrate the effectiveness of the proposed framework for matching multimodal images. CFOG performs best among the proposed similarity measures, followed by FHOG, FLSS and FSURF.

E. Computational Efficiency

A significant advantage of the proposed matching framework is its computational efficiency. Fig. 12 shows the run time of all similarity measures under the different template sizes. This experiment has been performed on an Intel Core i7-4710MQ 2.50GHz PC. Since MI requires computing the joint histogram for each matched window pair, it is the most time consuming among these similarity measures. All the proposed similarity measures outperform HOG_{ncc} because they accelerate the computation of similarity evaluation in the frequency domain by FFT, which is more efficient than the computation in the spatial domain.

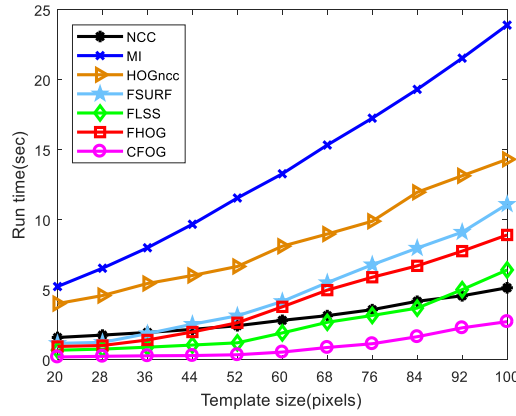


Fig. 12 Run times of all the similarity measures under different template sizes.

In the proposed matching framework, our similarity measures take different run times because they are based on different descriptors. The run time mostly depends on the time of calculating the descriptor. TABLE II gives the calculation time of the different descriptors for an image of 512×512 pixels. CFOG takes the least time for computing the descriptor. Accordingly, it spends the least run time among these similarity measures in the matching processing, followed by FLSS, FHOG, and FSURF. Moreover, CFOG also outperforms NCC in computational efficiency.

TABLE II
EXTRACTION TIME OF THE PROPOSED SIMILARITY MEASURES FOR AN IMAGE OF 512×512 PIXELS

| Similarity measure | Extraction time |
|--------------------|-----------------|
| FSURF | 2.905 sec |
| FHOG | 1.178 sec |
| FLSS | 0.693 sec |
| CFOG | 0.210 sec |

VI. Experimental Results: Performance of the Registration System

To validate the effectiveness of the automatic registration system based on the proposed matching framework (see Section VI), two popular commercial software systems (i.e. ENVI 5.0 and ERDAS 2013) are used for comparison. Both softwares have the function modules for automatic remote sensing image registration: “Image Registration Workflow (ENVI)” and “AutoSync (ERDAS)”. Considering that large-size remote sensing images are common in practice, we use a pair of multimodal images with more than $20,000 \times 20,000$ pixels in the experiment.

A. Datasets

A pair of very large-size SAR and optical images is used to compare our system with ENVI and ERDAS. Fig. 13 shows the test images and TABLE III provides their description. The challenges of registering the two images are as follows.

1) *Geometric distortions*: the images cover different terrains including mountain and plain areas, and have complex global and local geometric distortions between such images.

2) *Intensity differences*: significant non-linear intensity differences can be observed between the two images because they are captured by different sensors and in different spectral regions.

3) *Temporal differences*: the two images have a temporal difference of 12 months, which results in some changes occurred on the ground.

4) *Very large-size*: the SAR image and the optical image have the size of $29,530 \times 21,621$ pixels and $30,978 \times 30,978$ pixels, respectively.

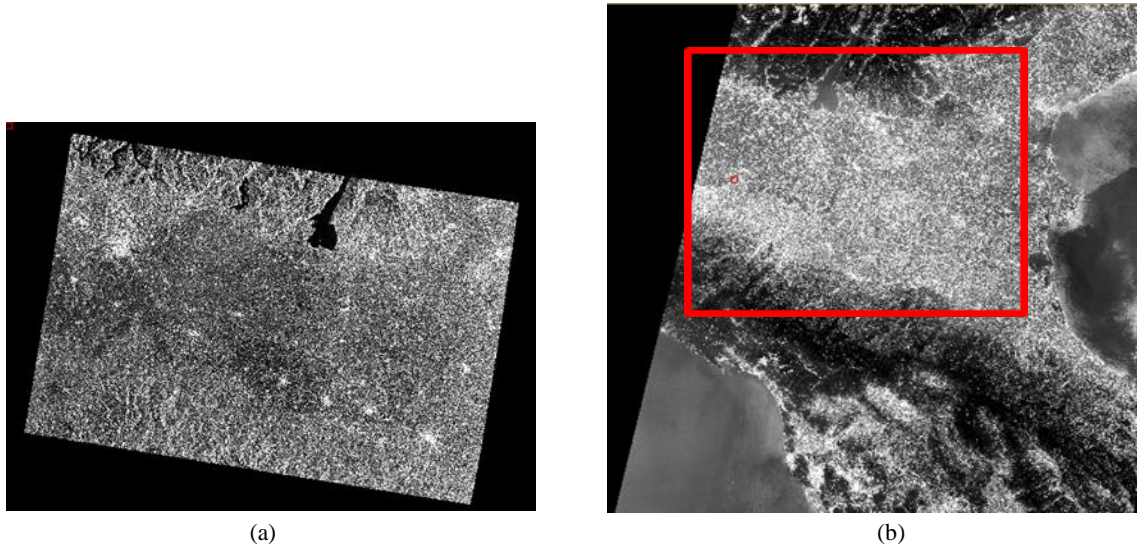


Fig. 13 Very large-size SAR and optical images. (a) SAR image. (b) Optical image. The red box highlights the overlapping area between the two images.

TABLE III
DESCRIPTIONS OF THE TEST IMAGES

| Characteristics | Reference image | Sensed image |
|-----------------|-----------------|--|
| Sensor | Sentinel-1 SAR | Sentinel-2 Multispectral (optical) Instrument band 1 |
| Resolution | 10m | 10m |
| Date | 07/2015 | 07/2016 |
| Size (pixels) | 29530×21621 | 30978×30978 |

B. Implementation details

To our best knowledge, both ENVI and EARDAS employ the template matching scheme to detect CPs between images, which is the same as that in our system. Accordingly, to make a fair comparison, all the three systems set the same parameters for image matching and use the piecewise linear transformation model for image rectification. For the similarity measures, ENVI achieves image matching by NCC and MI, which are referred as “ENVI-NCC” and “ENVI-MI” in this paper, respectively. ERDAS employs NCC to detect CPs, and uses a pyramid-based matching technique to enhance the robustness and computational efficiency. TABLE IV gives the parameters used in all the systems. It should be noted that because ERDAS uses the pyramid-based technique to guide the image matching, some parameters, such as the search and template window sizes, cannot be set too large. Instead, these parameters are set to the default values for ERDAS.

TABLE IV
PARAMETER SETTING IN ALL THE THREE SYSTEMS

| Parameter item | Proposed system | ENVI | ERDAS |
|--------------------------------------|-----------------|-----------------|---------|
| Number of detected interest points | 900 | 900 | 900 |
| Search window size | 80 | 80 ² | Default |
| Template window size | 80 | 80 | Default |
| RMSE Threshold for Outlier rejection | 3.5 pixels | 3.5 pixels | Default |

C. Analysis of Registration Results

We select 50 check points between the reference and registered images by the method described in Section V-B, and employ the RMSE to evaluate the registration accuracy. TABLE V reports the registration results for the three systems. The proposed system outperforms the others, achieving the most matched CPs, the least run time, and the highest registration accuracy.

TABLE V
REGISTRATION RESULTS OF THE THREE SYSTEMS

| Method | CPs | Run time (sec.) | RMSE (pixels) |
|------------------------|------------|-----------------|---------------|
| Before-registration | | | 18.65 |
| ENVI-NCC | 20 | 26.88 | 24.35(failed) |
| ENVI-MI | 88 | 458.89 | 4.58 |
| ERDAS | 56 | 301.68 | 14.20 |
| Proposed system | 303 | 19.98 | 2.31 |

ENVI-NCC fails because its registration accuracy is even worse than that of before-registration, while ENVI-MI and ERDAS improve the registration accuracy compared with before-registration. The proposed system not only achieves the higher registration accuracy, but also it is about 20 times and 15 times faster than ENVI-MI and ERDAS, respectively. Fig. 14 shows the registration results of before-registration, ERDAS, ENVI-MI, and the proposed system. One can clearly see that our system performs best, followed by ENVI-MI and ERDAS. The above experimental results show that the proposed system is effective for the registration of very large-size multimodal images, and outperforms ENVI and ERDAS in both registration accuracy and computational efficiency.

² Note: The “search window size” of our system is different from the “search window size” of ENVI. The former is the move range of the center pixel of template window, while the latter is equal to the sum of the move range and template window size. Therefore, it should be set to 160 pixels in the interface of ENVI.

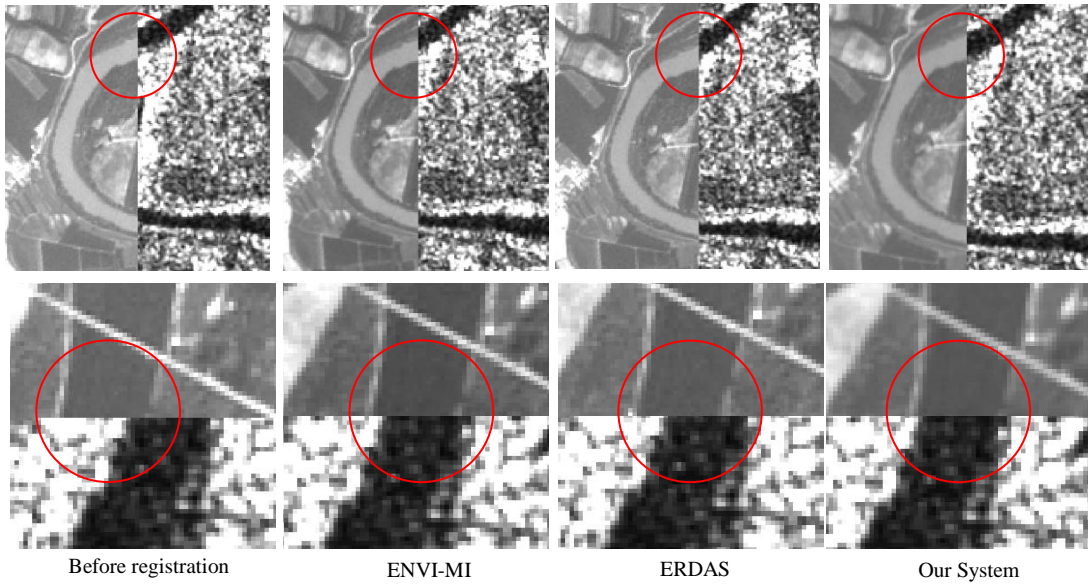
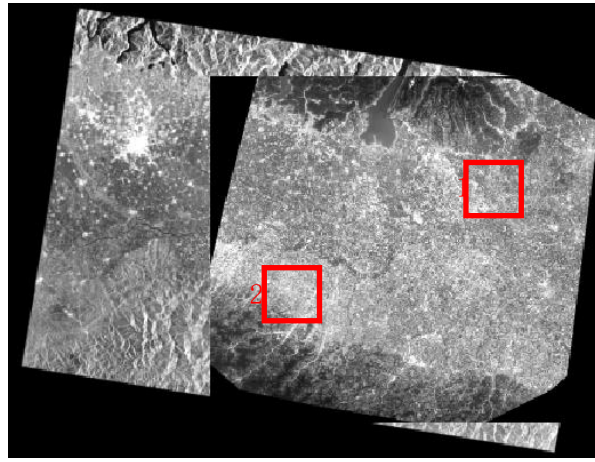


Fig. 14 Registration results of before-registration, ENVI-MI, ERDAS, and the proposed system. Line 2 shows the registration results in the overlapping area of SAR and optical images. Line 3 shows the registration results in box 1. Line 3 shows the registration results in box 2.

VII. Conclusions

This paper presents a fast and robust matching framework for registration of multimodal remote sensing images. It intends to address significant nonlinear intensity differences between such images. In the proposed framework, structures and shape properties of images are first captured by the pixel-wise feature representation. Then a similarity measure based on the pixel-wise feature representation is built in the frequency domain, using FFT to speed up the image matching task. Based on this framework, HOG, LSS, and SURF are integrated as similarity measures (named FHOG, FLSS, FSURF, respectively) for

CP detection. Moreover, a novel pixel-wise feature representation named CFOG is also proposed using orientated gradients of images. Ten various multimodal images, including optical, LiDAR, SAR, and map, are used to evaluate the proposed framework. The experimental results show that CFOG, FHOG, FLSS and FSURF outperform the state-of-the-art similarity measures such as NCC and MI in matching precision and achieve a computational efficiency comparable with NCC. Moreover, CFOG is faster than NCC. This demonstrates that the proposed framework is effective and robust for multimodal matching. In addition, an automatic image registration system is developed based on the proposed framework. The experimental results using a pair of very large-size SAR and optical images show that the proposed system outperforms ENVI and ERDAS commercial softwares in both registration accuracy and computational efficiency. Especially for computational efficiency, the proposed system is about 20 times faster than ENVI, and 15 times faster than ERDAS, respectively. This demonstrates that the proposed system has the potential for engineering application.

The proposed framework is general and can integrate different kinds of local descriptors for multimodal matching. Its performance depends on the local descriptors used to form the pixel-wise feature representation. Our experiments show that the descriptors based on the gradient orientation histogram (i.e, CFOG and FHOG) present relatively better performance, followed by FLSS and FSURF. When compared with FHOG, CFOG improves the matching performance, especially in computational efficiency by using the convolution with the Gaussian kernel instead of the trilinear interpolation to build the descriptor.

The main limitation of the proposed framework is that it cannot handle the images with large rotation and scale differences. In future works, we will attempt to integrate the local descriptors with rotation and scale invariance into the proposed framework for multimodal registration.

REFERENCE

- Bay, H., Ess, A., Tuytelaars, T., Van Gool, L., 2008. Speeded-up robust features (SURF). *Comput Vis Image Und*, 110 (3), 346-359.
- Belongie, S., Malik, J., Puzicha, J., 2002. Shape matching and object recognition using shape contexts. *IEEE Transactions on Pattern Analysis and Machine Intelligence*, 24 (4), 509-522.
- Bouchiha, R., Besbes, K., 2013. Automatic remote-sensing image registration using SURF. *International Journal of Computer Theory and Engineering*, 5 (1),

- Bracewell, R.N., Bracewell, R.N., 1986. The Fourier transform and its applications. McGraw-Hill New York.
- Brox, T., Malik, J., 2011. Large displacement optical flow: descriptor matching in variational motion estimation. *IEEE Transactions on Pattern Analysis and Machine Intelligence*, 33 (3), 500-513.
- Brunner, D., Lemoine, G., Bruzzone, L., 2010. Earthquake damage assessment of buildings using VHR optical and SAR imagery. *IEEE Transactions on Geoscience and Remote Sensing*, 48 (5), 2403-2420.
- Bruzzone, L., Bovolo, F., 2013. A novel framework for the design of change-detection systems for very-high-resolution remote sensing images. *Proceedings of the IEEE*, 101 (3), 609-630.
- Bunting, P., Labrosse, F., Lucas, R., 2010. A multi-resolution area-based technique for automatic multi-modal image registration. *Image Vision Comput*, 28 (8), 1203-1219.
- Chen, H.M., Arora, M.K., Varshney, P.K., 2003. Mutual information-based image registration for remote sensing data. *Int Journal Remote Sens*, 24 (18), 3701-3706.
- Chen, M., Shao, Z., 2013. Robust affine-invariant line matching for high resolution remote sensing images. *Photogrammetric Engineering & Remote Sensing*, 79 (8), 753-760.
- Cole-Rhodes, A.A., Johnson, K.L., LeMoigne, J., Zavorin, I., 2003. Multiresolution registration of remote sensing imagery by optimization of mutual information using a stochastic gradient. *IEEE Transactions Image Process*, 12 (12), 1495-1511.
- Dalal, N., Triggs, B., 2005. Histograms of oriented gradients for human detection, *Computer Vision and Pattern Recognition*, 2005. CVPR 2005, pp. 886-893.
- Fan, B., Huo, C., Pan, C., Kong, Q., 2013. Registration of optical and SAR satellite images by exploring the spatial relationship of the improved SIFT. *IEEE Geoscience and Remote Sensing Letters*, 10 (4), 657-661.
- Fan, X.F., Rhody, H., Saber, E., 2010. A Spatial-Feature-Enhanced MMI Algorithm for Multimodal Airborne Image Registration. *IEEE Transactions on Geoscience and Remote Sensing*, 48 (6), 2580-2589.
- Fitch, A., Kadyrov, A., Christmas, W.J., Kittler, J., 2002. Orientation Correlation, *BMVC 2002*, pp. 1-10.
- Gesto-Diaz, M., Tombari, F., Gonzalez-Aguilera, D., Lopez-Fernandez, L., Rodriguez-Gonzalez, P., 2017. Feature matching evaluation for multimodal correspondence. *ISPRS Journal of Photogrammetry and Remote Sensing*, 129, 179-188.
- Goncalves, H., Corte-Real, L., Goncalves, J.A., 2011. Automatic image registration through image segmentation and SIFT. *IEEE Transactions on Geoscience and Remote Sensing*, 49 (7), 2589-2600.
- Goncalves, H., Goncalves, J.A., Corte-Real, L., Teodoro, A.C., 2012. CHAIR: automatic image registration based on correlation and Hough transform. *Int Journal of Remote Sens*, 33 (24), 7936-7968.
- Heinrich, M.P., Jenkinson, M., Bhushan, M., Matin, T., Gleeson, F.V., Brady, S.M., Schnabel, J.A., 2012. MIND: Modality independent neighbourhood descriptor for multi-modal deformable registration. *Medical Image Analysis*, 16 (7), 1423-1435.
- Hel-Or, Y., Hel-Or, H., David, E., 2014. Matching by Tone Mapping: Photometric Invariant Template Matching. *IEEE Transactions on Pattern Analysis and Machine Intelligence*, 36 (2), 317-330.
- Huang, L., Li, Z., 2010. Feature-based image registration using the shape context. *International Journal of Remote Sensing*, 31 (8), 2169-2177.
- Huo, C., Pan, C., Huo, L., Zhou, Z., 2012. Multilevel SIFT Matching for Large-Size VHR Image Registration. *IEEE Geoscience and Remote Sensing Letters*, 9 (2), 171-175.
- Kelman, A., Sofka, M., Stewart, C.V., 2007. Keypoint descriptors for matching across multiple image modalities and non-linear intensity variations, *CVPR 2007*, pp. 3257-3263.
- Lazebnik, S., Schmid, C., Ponce, J., 2006. Beyond bags of features: Spatial pyramid matching for recognizing natural scene categories, *CVPR 2006*, pp. 2169-2178
- Li, H., Manjunath, B., Mitra, S.K., 1995. A contour-based approach to multisensor image registration. *IEEE Transactions on Image Processing*, 4 (3), 320-334.
- Li, Z., Mahapatra, D., Tielbeek, J.A.W., Stoker, J., van Vliet, L.J., Vos, F.M., 2016. Image Registration Based on Autocorrelation of Local Structure. *IEEE Trans Med Imaging*, 35 (1), 63-75.
- Liu, C., Yuen, J., Torralba, A., 2011. Sift flow: Dense correspondence across scenes and its applications. *IEEE Transactions on Pattern Analysis and Machine Intelligence*, 33 (5), 978-994.
- Lowe, D.G., 2004. Distinctive image features from scale-invariant keypoints. *International Journal of Computer Vision*, 60 (2), 91-110.

- Ma, J., Zhou, H., Zhao, J., Gao, Y., Jiang, J., Tian, J., 2015. Robust feature matching for remote sensing image registration via locally linear transforming. *Ieee T Geosci Remote*, 53 (12), 6469-6481.
- Ma, J.L., Chan, J.C.W., Canters, F., 2010. Fully Automatic Subpixel Image Registration of Multiangle CHRIS/Proba Data. *IEEE Transactions on Geoscience and Remote Sensing*, 48 (7), 2829-2839.
- Murphy, J.M., Le Moigne, J., Harding, D.J., 2016. Automatic Image Registration of Multimodal Remotely Sensed Data With Global Shearlet Features. *IEEE Transactions on Geoscience and Remote Sensing*, 54 (3), 1685-1704.
- Ravanbakhsh, M., Fraser, C.S., 2013. A comparative study of DEM registration approaches. *Journal of Spatial Science*, 58 (1), 79-89.
- Reddy, B.S., Chatterji, B.N., 1996. An FFT-based technique for translation, rotation, and scale-invariant image registration. *IEEE Transactions Image Process*, 5 (8), 1266-1271.
- Rivaz, H., Karimaghloo, Z., Collins, D.L., 2014. Self-similarity weighted mutual information: A new nonrigid image registration metric. *Medical Image Analysis*, 18 (2), 343-358.
- Sedaghat, A., Ebadi, H., 2015. Remote Sensing Image Matching Based on Adaptive Binning SIFT Descriptor. *IEEE Transactions on Geoscience and Remote Sensing*, 53 (10), 5283-5293.
- Sedaghat, A., Mokhtarzade, M., Ebadi, H., 2011. Uniform Robust Scale-Invariant Feature Matching for Optical Remote Sensing Images. *IEEE Transactions on Geoscience and Remote Sensing*, 49 (11), 4516-4527.
- Shechtman, E., Irani, M., 2007. Matching local self-similarities across images and videos, *CVPR 2007*, pp. 1-8.
- Suri, S., Reinartz, P., 2010. Mutual-Information-Based Registration of TerraSAR-X and Ikonos Imagery in Urban Areas. *IEEE Transactions on Geoscience and Remote Sensing*, 48 (2), 939-949.
- Teke, M., Temizel, A., 2010. Multi-spectral satellite image registration using scale-restricted SURF, *ICPR 2010*, pp. 2310-2313.
- Tola, E., Lepetit, V., Fua, P., 2010. Daisy: An efficient dense descriptor applied to wide-baseline stereo. *IEEE Transactions on Pattern Analysis and Machine Intelligence*, 32 (5), 815-830.
- Tuia, D., Marcos, D., Camps-Valls, G., 2016. Multi-temporal and multi-source remote sensing image classification by nonlinear relative normalization. *ISPRS Journal of Photogrammetry and Remote Sensing*, 120, 1-12.
- Uss, M.L., Vozel, B., Lukin, V.V., Chehdi, K., 2016. Multimodal Remote Sensing Image Registration With Accuracy Estimation at Local and Global Scales. *IEEE Transactions on Pattern Analysis and Machine Intelligence*, 54 (11), 6587-6605.
- Viola, P., Jones, M., 2001. Rapid object detection using a boosted cascade of simple features, *Computer Vision and Pattern Recognition, 2001. CVPR 2001*, pp. I-511-I-518.
- Wan, X., Liu, J., Yan, H., Morgan, G.L., 2016. Illumination-invariant image matching for autonomous UAV localisation based on optical sensing. *ISPRS Journal of Photogrammetry and Remote Sensing*, 119, 198-213.
- Wan, X., Liu, J.G., Yan, H., 2015. The Illumination Robustness of Phase Correlation for Image Alignment. *IEEE Transactions on Pattern Analysis and Machine Intelligence*, 53 (10), 5746-5759.
- Wong, A., Orchard, J., 2008. Efficient FFT-accelerated approach to invariant optical-LIDAR registration. *IEEE Transactions on Geoscience and Remote Sensing*, 46 (11), 3917-3925.
- Xu, X., Li, X., Liu, X., Shen, H., Shi, Q., 2016. Multimodal registration of remotely sensed images based on Jeffrey's divergence. *ISPRS Journal of Photogrammetry and Remote Sensing*, 122, 97-115.
- Ye, Y., 2017. Fast and Robust Registration of Multimodal Remote Sensing Images via Dense Orientated Gradient Feature, *International Archives of the Photogrammetry, Remote Sensing & Spatial Information Sciences, ISPRS Geospatial Week 2017*
- Ye, Y., Bruzzone, L., Shan, J., Shen, L., 2017a. Fast and Robust Structure-based Multimodal Geospatial Image Matching, *IGARSS 2017*, in press.
- Ye, Y., Shan, J., 2014. A local descriptor based registration method for multispectral remote sensing images with non-linear intensity differences. *ISPRS Journal of Photogrammetry and Remote Sensing*, 90, 83-95.
- Ye, Y., Shan, J., Bruzzone, L., Shen, L., 2017b. Robust registration of multimodal remote sensing images based on structural similarity. *IEEE Transactions on Geoscience and Remote Sensing*, 55 (5), 2941-2958.
- Ye, Y., Shen, L., 2016. Hopc: a Novel Similarity Metric Based on Geometric Structural Properties for Multi-Modal Remote Sensing Image Matching. *ISPRS Annals of Photogrammetry, Remote Sensing and Spatial Information Sciences, ISPRS Congress 2016*, pp. 9-16.
- Ye, Y., Shen, L., Hao, M., Wang, J., Xu, Z., 2017c. Robust optical-to-SAR image matching based on shape properties. *Ieee Geosci Remote S*, 14 (4), 564-568.
- Ye, Y., Shen, L., Wang, J., Li, Z., Xu, Z., 2015. Automatic matching of optical and SAR imagery through shape property, *IGARSS 2015*, pp. 1072-1075.

- Yu, L., Zhang, D.R., Holden, E.J., 2008. A fast and fully automatic registration approach based on point features for multi-source remote-sensing images. *Comput Geosci-Uk*, 34 (7), 838-848.
- Zavorin, I., Le Moigne, J., 2005. Use of multiresolution wavelet feature pyramids for automatic registration of multisensor imagery. *Ieee T Image Process*, 14 (6), 770-782.
- Zhang, Y., 2004. Understanding image fusion. *Photogrammetric engineering and remote sensing*, 70 (6), 657-661.
- Zitova, B., Flusser, J., 2003. Image registration methods: a survey. *Image and Vision Computing*, 21 (11), 977-1000.